

# CrystEngComm

Accepted Manuscript



This is an *Accepted Manuscript*, which has been through the Royal Society of Chemistry peer review process and has been accepted for publication.

*Accepted Manuscripts* are published online shortly after acceptance, before technical editing, formatting and proof reading. Using this free service, authors can make their results available to the community, in citable form, before we publish the edited article. We will replace this *Accepted Manuscript* with the edited and formatted *Advance Article* as soon as it is available.

You can find more information about *Accepted Manuscripts* in the [Information for Authors](#).

Please note that technical editing may introduce minor changes to the text and/or graphics, which may alter content. The journal's standard [Terms & Conditions](#) and the [Ethical guidelines](#) still apply. In no event shall the Royal Society of Chemistry be held responsible for any errors or omissions in this *Accepted Manuscript* or any consequences arising from the use of any information it contains.

# The nature of the C-Br...Br-C intermolecular interactions found in molecular crystals: A general theoretical-database study

Marçal Capdevila-Cortada <sup>a,b</sup> and Juan J. Novoa <sup>\*a</sup>

<sup>a</sup> Departament de Química Física and IQTCUB, Facultat de Química, Universitat de Barcelona, Av. Diagonal 645, 08028 Barcelona (Spain)

<sup>b</sup> Current address: Institute of Chemical Research of Catalonia (ICIQ), Av. Països Catalans 16, 43007 Tarragona (Spain)

E-mail: juan.novoa@ub.edu

Electronic supplementary information (ESI) available: Distance and angle distribution of all dimers extracted from the CSD. Cartesian coordinates of all optimized dimers.

**ABSTRACT:** The nature of the C-Br...Br-C intermolecular interactions has been evaluated by doing first-principles calculations on model dimers and on full-size dimers extracted from crystals deposited in the Cambridge Structural Database presenting short-distance C-Br...Br-C contacts. First of all, the strength of the C(sp<sup>n</sup>)-Br...Br-C(sp<sup>n</sup>) interaction was determined at the MP2/CBS level on model dimers placed at their most stable orientation, getting values of -1.72, -1.83, and -1.91 kcal mol<sup>-1</sup> for n = 3, 2 (non-aromatic), and 1, respectively. SAPT analyses of the interaction energy showed that it is dominated by the dispersion term, although a strong electrostatic component is also present, which depends on the fragments dipole moment (induced by the substituents attached to the two C atoms involved in the C-Br...Br-C interaction) and the  $\sigma$ -hole of the halogen atoms (induced by the asymmetry of the electron density around each bromine atom). The angular dependence of the C-Br...Br-C interactions was determined by computing the  $E_{\text{int}}(\theta_1, \theta_2)$  surface (where  $\theta_1$  and  $\theta_2$  are the  $\langle \text{C-Br}\dots\text{Br} \rangle$  and  $\langle \text{Br}\dots\text{Br-C} \rangle$  angles) for the (CH<sub>3</sub>Br)<sub>2</sub> dimer. The most stable orientations were found at  $\theta_1 \square \square \square \theta_2 = 90^\circ$  (a case of Type I orientation) and at  $\theta_1 \approx 180^\circ$  and  $\theta_2 \approx 90^\circ$  (Type II orientation). The  $E_{\text{int}}(\theta_1, \theta_2)$  surface also showed that the  $\theta_1 \square \square \square \theta_2 = 150^\circ$  orientation is that with the lowest energy among all Type I, but rather than a minimum, it should be considered as a saddle point between both Type II minimum energy orientations. Finally, in order to gain information of the properties of the C-Br...Br-C interactions in real cases, the interaction energy was evaluated for 39 dimers extracted from the Cambridge Structural Database that present C-Br...Br-C interactions smoothly distributed over the 3.0 – 4.5 Å range. This allowed establishing the overall stabilizing nature of these interactions in complex molecules (all have interaction energies range from -2.35 to -0.38 kcal mol<sup>-1</sup>, with an average value of -1.26 kcal mol<sup>-1</sup>). The correlation between stronger interaction energies and higher electron density values at the Br...Br bond critical point was shown to be incorrect for sub-van der Waals C-Br...Br-C interactions.

## INTRODUCTION

The control of non-covalent interactions has been proven to be a crucial factor in the rational design of molecular solids.<sup>1,2</sup> Among the growing list of non-covalent interactions commonly reported to exist in molecular crystals, which includes as its most prominent members hydrogen bonds (A-H...B),<sup>3-8</sup> halogen bonds (A-X...B),<sup>9,10</sup> and stacking (also called  $\pi$ - $\pi$ ) interactions,<sup>11-13</sup> halogen...halogen interactions (represented as X...X, or C-X...X-C, where X is a halogen atom) were long ago identified as a key driving force controlling the packing of halogen-containing crystals.<sup>14-23</sup> Early theoretical studies investigated the origin of the stabilizing character of X...X interactions, which was finally ascribed to the presence of a region of positive electrostatic potential around the halogen atom, the so-called  $\sigma$ -hole,<sup>24</sup> caused by the asymmetry of its electron density.<sup>17,25-28</sup>

The strength of X...X interactions was generally found to depend on the halogen atom as follows: I > Br > Cl > F.<sup>19</sup> The hybridization of the carbon atom to which the halogen is covalently bonded (the *ipso* carbon, C(*ipso*)) was also found to affect the strength of the interaction, which decreases according to the following order: C(sp<sup>2</sup>) > C(sp) > C(sp<sup>3</sup>).<sup>19</sup> Previous studies showed the presence of two preferred orientations for C-X...X-C interactions, commonly known as Type I and Type II orientations.<sup>17</sup> The former occur when  $\theta_1 = \theta_2$  (where  $\theta_1$  and  $\theta_2$  refer to the  $\langle \text{C-X}_1\dots\text{X}_2 \rangle$  and  $\langle \text{X}_1\dots\text{X}_2\text{-C} \rangle$  angles), while the latter are found when  $\theta_1 \approx 180^\circ$  and  $\theta_2 \approx 90^\circ$  (or, equivalently, when  $\theta_2 \approx 180^\circ$  and  $\theta_1 \approx 90^\circ$ ). Type I interactions are known to present a maximum of probability around 140-160° and are usually obtained in crystals presenting inversion centers and symmetry planes, while Type II interactions are usually associated with screw axis and glide planes. The existence of Type I and Type II orientations has been explained in terms of the  $\sigma$ -hole properties.<sup>29</sup> Specific analyses of the electron density recently provided more insights on this subject.<sup>20,30,31</sup> In particular, Vener and coworkers reported a correlation between the topology of the electron density

and the strength of Cl...Cl interactions for contacts larger than twice the chlorine van der Waals radii,<sup>30</sup> although this correlation was found to fail for contacts whose distance is shorter than such threshold.<sup>32</sup>

As part of a general project aimed at obtaining an accurate determination of the properties of the C-X...X-C interactions present in molecular crystals based on first principles theoretical computations, herein we report the results concerning the exhaustive evaluation of the nature of the C-Br...Br-C interactions. This work extends two previous studies of this kind in C-F...F-C and C-Cl...Cl-C interactions.<sup>32,33</sup> The study here reported combines MP2 interaction energy computations and SAPT calculations about the nature of the interaction energy. Some of these results were obtained on model dimers, while others were obtained on full-size dimers extracted from the Cambridge Structural Database (CSD). After assessing on model dimers the computational methodology used throughout the work, the results describing the characteristic properties of the C-Br...Br-C interactions are presented in the following order: (a) determination of the interaction energy curves for the (CBr<sub>4</sub>)<sub>2</sub> dimer, evaluating their dependence on the number and relative orientation of Br...Br contacts; (b) study of the properties of the C-Br...Br-C interactions found in the CBr<sub>4</sub> crystal; (c) importance of the electrostatic component in the C-Br...Br-C interactions, evaluated on (CH<sub>4-n</sub>Br<sub>n</sub>)<sub>2</sub> dimers when n = 1 – 4 (n = degree of bromo-substitution); (d) determination of the angular dependence of the C-Br...Br-C interactions, studied for the (CH<sub>3</sub>Br)<sub>2</sub> model dimer; (e) importance of the C(*ipso*) hybridization, investigated on dimers of bromo-substituted methane, ethylene, benzene, and acetylene; and (f) evaluation of the properties of the C-Br...Br-C interactions in 39 full-sized dimers extracted from published molecular crystals collected in the CSD that present one C-Br...Br-C interaction smoothly distributed over the 3.0 – 4.5 Å range.

## METHODOLOGY

The nature of the halogen...halogen interactions is commonly ascribed to the dispersion component of the interaction energy, although accepting the presence of a small electrostatic component.<sup>28</sup> The dominance of the dispersive component mostly originates from the presence of many short-distance halogen...halogen contacts where (lone pair)...(lone pair) overlaps are produced among the interacting halogen atoms. The interaction energy of dimers presenting halogen...halogen interactions was evaluated in this work by doing MP2 calculations. The MP2 method accounts for a high percentile of the electron correlation of a monomer and dimer, in a reasonable amount of cpu time and other computational resources. It also provided good results in recent studies of non-covalent interactions involving halogen atoms.<sup>19,32,33,44,45</sup> Thus, all interaction energy evaluations were carried out at the MP2 level.

In these MP2 calculations, the aug-cc-pVTZ basis set was used in the CBr<sub>4</sub> molecular crystal and all other model dimer calculations, whereas the aug-cc-pVDZ basis set was employed in the calculations involving dimers from crystals extracted from the Cambridge Structural Database (CSD). The values obtained using these two basis sets were compared against MP2 interaction energy obtained for the complete basis set (CBS), for three model dimers placed in three different orientations. The CBS results were obtained by applying the Helgaker extrapolation<sup>34,35</sup> to the MP2/aug-cc-pVXZ (X = D, T, Q, 5) interaction energies. The evaluation of the E<sub>int</sub>(θ<sub>1</sub>, θ<sub>2</sub>) potential energy surface was carried out at the MP2/6-311++G\*\* level. All geometry optimizations were performed at the MP2/aug-cc-pVDZ level, and the potential energy curves and surfaces were obtained after optimizing the geometries for all remaining variables. For all reported interaction energies, the Basis Set Superposition Error (BSSE) was corrected using the Counterpoise (CP) approach.<sup>36</sup> All the previous calculations were done using the Gaussian03 package.<sup>37</sup>

The nature of the interaction energy was also quantitatively determined by running Symmetry Adapted Perturbation Theory (SAPT) calculations.<sup>38</sup> According to the SAPT methodology, the interaction energy can be decomposed into the sum of four components: the electrostatic (E<sub>el</sub>), exchange-repulsion (E<sub>ex</sub>), induction (E<sub>ind</sub>), and dispersion (E<sub>disp</sub>) components, as specified in the literature.<sup>33,39</sup>

$$E_{\text{int}} = E_{\text{el}} + E_{\text{ex}} + E_{\text{ind}} + E_{\text{disp}} \quad (1)$$

The SAPT2 level of the SAPT algorithm was chosen in these decompositions. In all cases, the sum of these components gives E<sub>int</sub> values nearly identical to those from the MP2 calculations. These SAPT calculations were carried out using the aug-cc-pVTZ basis set for the interacting bromine atoms, the aug-cc-pVDZ for the remaining bromine atoms, and the cc-pVDZ for all other atoms. All SAPT calculations were done using the SAPT2008 program.<sup>40</sup>

The Atoms-In-Molecules (AIM) methodology<sup>41</sup> was used to characterize the intermolecular bonds. These calculations were done using an in-house version of the PROAIM program.<sup>42</sup> According to Bader's AIM theory,<sup>41</sup> intermolecular bonds are associated with a (3,-1) bond critical point (BCP) in the electron density, that is, a point where the gradient of the density is zero and the second derivative matrix has two negative and one positive eigenvalues (curvatures). Any BCP can be characterized giving its density (ρ) and the sum of its curvatures (∇<sup>2</sup>ρ).

The search for dimers in molecular crystals published in the literature, and presenting only one C-Br...Br-C intermolecular short-distance contact, was carried out by looking for those crystals in version 5.35, November 2013 update of the CSD, released by the Cambridge Crystallographic Data Centre (CCDC).<sup>43</sup> The following filters were applied: 3D coordinates determined, not disorder, no errors, not polymeric, no powder structures, and a crystallographic R factor ≤ 0.05. The search was done within the 3.0 – 4.5 Å range of distances. The selected dimers present a Br...Br distance smoothly distributed within such a range of distances. The values of their θ<sub>1</sub> and θ<sub>2</sub> angles and the hybridization of their C(*ipso*) atoms were also measured, for their accounting.

## RESULTS AND DISCUSSION

### 1. Assessment of the computational methodology

The accuracy of the chosen computational methodology was assessed by comparing the BSSE-corrected MP2/aug-cc-pVDZ and MP2/aug-cc-pVTZ interaction energies computed for the  $(\text{CH}_3\text{Br})_2$ ,  $(\text{H}_2\text{CCHBr})_2$ , and  $(\text{HCCBr})_2$  model dimers with the MP2/CBS limit result,<sup>34,35</sup> Figure 1. These comparisons were done for three relative orientations of each dimer, namely (180,180), (180,90), and (90,90), defined following the  $(\theta_1, \theta_2)$  notation (where the  $\theta_1$  and  $\theta_2$  angles are defined as  $\langle \text{C-X}_1 \cdots \text{X}_2 \rangle$  and  $\langle \text{X}_1 \cdots \text{X}_2 - \text{C} \rangle$ ). As shown in Figure 1, the three orientations of the three dimers show the same trends: (a) in all dimers the MP2/aug-cc-pVDZ interaction energy is  $\sim 0.6 \text{ kcal mol}^{-1}$  weaker than the CBS result, difference that becomes  $\sim 0.2 \text{ kcal mol}^{-1}$  at the MP2/aug-cc-pVTZ level; and (b) the most stable orientation, for all dimers and basis sets, is the (180,90) orientation. At the (180,90) orientation, the MP2/CBS interaction energy of each dimer is  $-1.72 \text{ kcal mol}^{-1}$  for  $(\text{CH}_3\text{Br})_2$ ,  $-1.83 \text{ kcal mol}^{-1}$  for  $(\text{H}_2\text{CCHBr})_2$ , and  $-1.91 \text{ kcal mol}^{-1}$  for  $(\text{HCCBr})_2$ . These interaction energies can be taken as benchmark values for the strength of the C-Br $\cdots$ Br-C interactions for each hybridization. At the light of these results, the aug-cc-pVTZ basis set was chosen for all the small dimer computations of Sections 1-5, while the aug-cc-pVDZ bases set was selected for the full-size dimers extracted from crystals, Section 6.

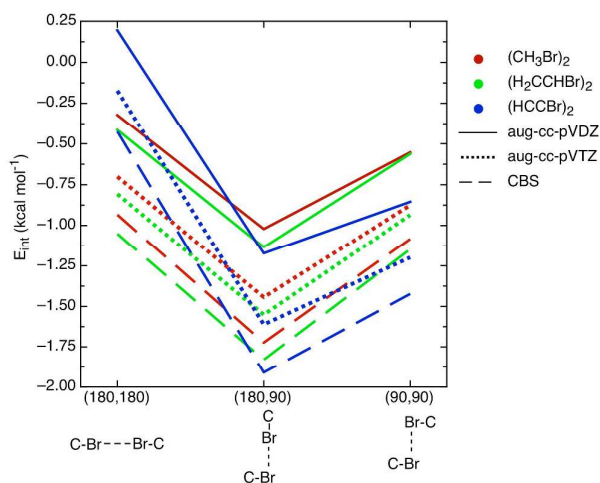


**Figure 1.** Interaction energies of the  $(\text{CH}_3\text{Br})_2$ ,  $(\text{H}_2\text{CCHBr})_2$ , and  $(\text{HCCBr})_2$  dimers obtained at the MP2 level using the aug-cc-pVDZ and aug-cc-pVTZ basis sets and the CBS limit extrapolation. These calculations were done for the three relative orientations shown below the horizontal axis, in each case at the optimum MP2/aug-cc-pVDZ geometry of the dimer at the given orientation.

### 2. The nature of the C-Br $\cdots$ Br-C interactions in $(\text{CBr}_4)_2$ dimers

$\text{CBr}_4$  is a neutral molecule that has neither a dipole nor a quadrupole moment. Therefore, at any given orientation of the  $(\text{CBr}_4)_2$  dimer, the dispersion component is expected to be the dominant attractive component in the dimer interaction energy, thus turning this system a good prototype to study the nature of the C-Br $\cdots$ Br-C interactions in their dispersion-dominated limit.

Among all possible geometrical arrangements of C-Br $\cdots$ Br-C interactions in  $(\text{CBr}_4)_2$  dimers, the six orientations shown in Figure 2 were considered as relevant limiting cases for the study of the properties of these interactions. They were identified using a  $(x:y)$  notation, which indicates the number of bromine atoms presenting short-distance contacts in both interacting molecules,  $x$  being those from the first molecule, and  $y$  that from the second fragment. There are cases where the dimer presents only one short-distance Br $\cdots$ Br contact (as in the (1:1) dimer), and others where six short-distance Br $\cdots$ Br contacts are found (as in the (3:3 sta) dimer). The number of these Br $\cdots$ Br short-distance contacts that are Br $\cdots$ Br bonds can be quantitatively determined by doing an AIM analysis of each dimer wavefunction, at the optimum geometry of the dimer (see Figure 2, where the position of all Br $\cdots$ Br (3,-1) bond critical points found in each dimer are plotted).

The interaction energy curve for the six dimers of Figure 2 was obtained by varying the separation between the fragments while preserving their relative orientation as that in Figure 2. All curves present a minimum more stable than their dissociated fragments. The (3:3 sta) orientation is the most stable one, with a minimum of  $-3.9 \text{ kcal mol}^{-1}$  at  $4.1 \text{ \AA}$ . The (3:1), (2:1), and (3:3 ecl) exhibit a minimum around  $-2.7 \text{ kcal mol}^{-1}$  at  $3.9$ ,  $3.75$ , and  $4.2 \text{ \AA}$ , respectively. The (2:2) and (1:1) curves are less stable (around  $-1.6$  and  $-1.0 \text{ kcal mol}^{-1}$ , respectively), and provide a minimum at  $3.7$  and  $4.0 \text{ \AA}$ . The most stable curve, (3:3 sta), exhibits six BCP, while the least stable, (1:1), exhibits only one. In general, the higher number of intermolecular contacts the larger the stabilization is, although such correlation is not always obeyed. Thus, the (2:1) minimum is  $1.1 \text{ kcal mol}^{-1}$  more stable than the (2:2) minimum, albeit the latter possesses two BCP. Similarly, the (3:3 sta) orientation, which presents six Br $\cdots$ Br interactions, exhibits a strength of  $-0.65 \text{ kcal mol}^{-1}$  per interaction, whereas the strength per interaction in the (2:1) dimer is  $-1.35 \text{ kcal mol}^{-1}$ . This indicates that the number of Br $\cdots$ Br contacts is not the only factor determining the strength of a dimer, thus suggesting that the angular orientation of the C-Br $\cdots$ Br-C contacts is also an important factor. Such finding is in good agreement with the variations observed in Figure 1, as also reported in the literature.<sup>32,44,46</sup>

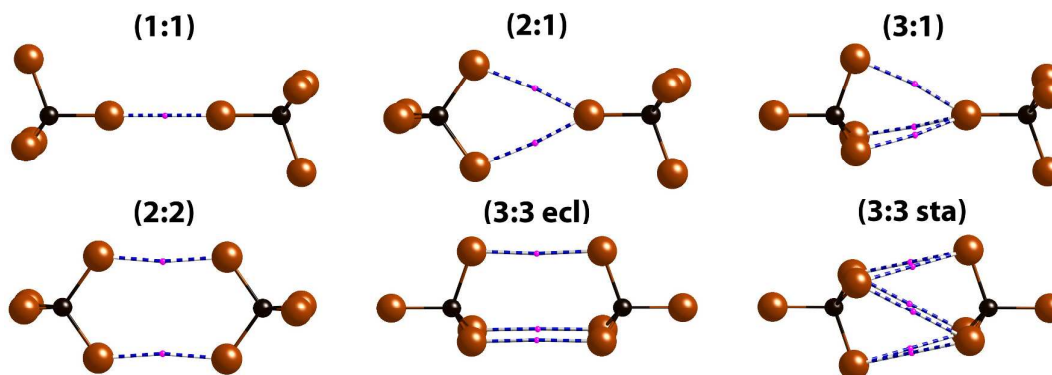


**Figure 2.** The six model orientations considered for the  $(\text{CBr}_4)_2$  dimer, all being local minima (at the MP2/aug-cc-pVDZ level) on the potential energy surface of the  $(\text{CBr}_4)_2$  dimer. The bond critical points at their equilibrium distance resulting from an AIM analysis of the wavefunction (obtained at the MP2/aug-cc-pVTZ level) are also shown.

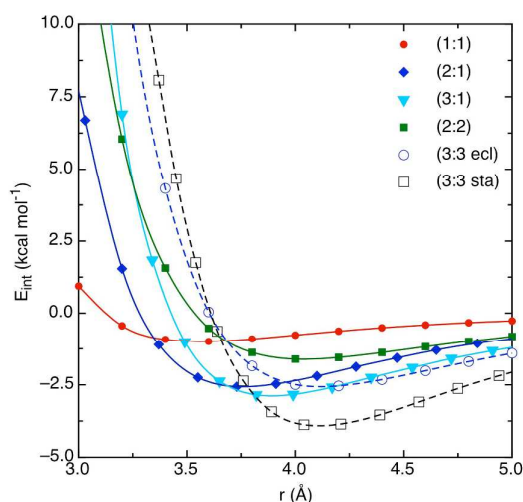


**Figure 3.** Interaction energy curves obtained at the MP2/aug-cc-pVTZ level, for the six  $(\text{CBr}_4)_2$  model dimers of Figure 2. The BSSE is corrected. The distance  $r$  is defined as the shortest  $\text{Br}\cdots\text{Br}$  distance.

Using the information about the six model dimers of Figure 2 we tried to analyze the packing of the room temperature polymorph of the  $\text{CBr}_4$  crystal (Figure 4, Refcode CTBROM06). This crystal packs in the  $C2/c$  space group and presents an unusually high number of molecules in the unit cell ( $Z=32$ ) and in the asymmetric unit ( $Z'=4$ ). There are 81  $\text{Br}\cdots\text{Br}$  intermolecular contacts within the 3.0 – 4.5 Å range, which can be grouped into the six categories of non-equivalent  $(\text{CBr}_4)_2$  dimers shown in Figure 5, **A** – **F**. Taking into account their relative orientation and the number of bonds (identified by doing an AIM analysis), one finds a correlation between the **A** – **F** dimers of Figure 5 and those shown in Figure 2: **A** and **B** dimers in Figure 5 are of the (2:1) type, **C** dimers are of the (3:3 ecl) type, **D** dimers correspond to the (3:2) dimers, **E** dimers are of the (3:3 sta) type, and **F** dimers correspond to the (2:2) type. Table 1 collects the interaction energy of these **A** – **F** dimers and the characteristic properties of their BCP. The (3:3 sta) dimer (**E**) exhibits the strongest interaction energy, followed by the (3:3 ecl) and the (3:2) interactions. The **A** and **B** interactions are of the (2:1) type, but since the  $\text{Br}\cdots\text{Br}$  distances are closer to the minimum of the (2:1) curve in **A** (Figure 3), its interaction energy is slightly stronger (0.3 kcal mol<sup>-1</sup>). At the same time, as shown in Figure 3, the **F** dimer (a (2:2) contact) is less stable than the **A** and **B** dimers, both (2:1) contacts. Notice, however, that the geometry of **F** in Figure 3 is far from the optimum geometry of the (2:2) dimer plotted in Figure 2, a fact that calls our attention on the relevance of the relative orientation in the strength of the dimer. All relative orientations except the (3:2) were previously considered in the model interactions of Figure 2, a fact that suggests that these orientations include all the likely relative orientations of the  $\text{C}-\text{Br}\cdots\text{Br}-\text{C}$  contacts present in dispersion-dominated molecular crystals.

The nature of the  $\text{C}-\text{Br}\cdots\text{Br}-\text{C}$  interactions in the  $(\text{CBr}_4)_2$  dimers was also quantitatively determined by looking at the dominant components of the interaction energy, which here were evaluated by doing a SAPT decomposition analysis of the (1:1) dimer at its optimum geometry (Table 2, first row). The similarity between the value of the interaction energy obtained by adding the SAPT components and the MP2 interaction energy (-1.04 and -0.98 kcal mol<sup>-1</sup>, respectively), illustrates the goodness of the SAPT decomposition. The dispersion component is found to be the dominant attractive component of the interaction energy ( $E_{\text{disp}} = -2.96$  kcal mol<sup>-1</sup>), while the electrostatic and

induction terms are 0.10 and  $-0.69 \text{ kcal mol}^{-1}$ , respectively. The exchange-repulsion component is strongly destabilizing ( $2.51 \text{ kcal mol}^{-1}$ ) and almost compensates the stabilizing dispersion component. The important role played by the exchange-repulsion component here is consistent with the findings of Dunitz and Gavezzotti, obtained from crystal packing considerations.<sup>47</sup>

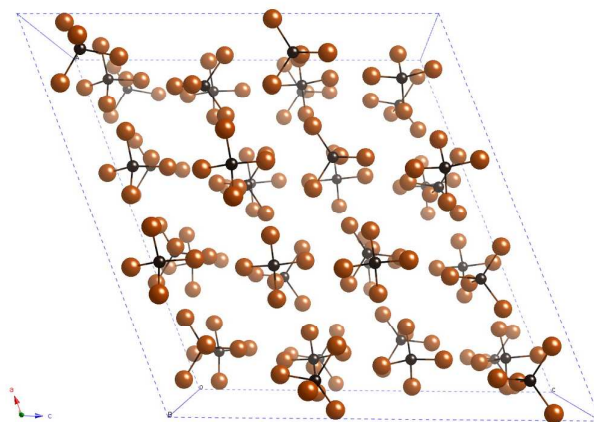


Figure 4. Unit cell of the  $\text{CBr}_4$  crystal (CSD Refcode: CTBROM06).

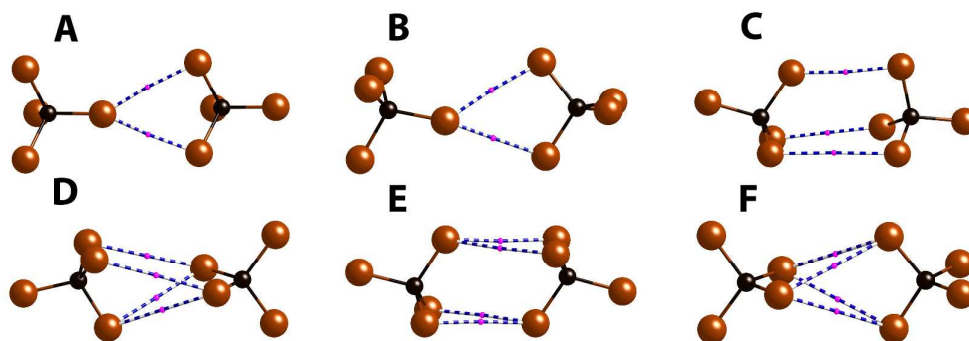


Figure 5. Orientation of the six non-equivalent dimers present in the  $\text{CBr}_4$  crystal. Their bond critical points resulting from an AIM analysis of the wavefunction (obtained at the MP2/aug-cc-pVTZ level) are also shown.

Table 1. Interaction energy of the six non-equivalent dimers present in the  $\text{CBr}_4$  crystal (see Figure 5). The calculations were done at the MP2/aug-cc-pVTZ level, correcting the BSSE. For each dimer, the density and Laplacian of all intermolecular  $\text{Br}\cdots\text{Br}$  BCPs are also collected.

dimer	contact	$E_{\text{int}}$ ( $\text{kcal mol}^{-1}$ )	$r$ ( $\text{\AA}$ )	$\rho$ (a.u.)	$\nabla^2 \rho$ (a.u.)
A	(2:1)	-2.66	3.777	$6.4 \cdot 10^{-3}$	0.017
			3.623	$8.1 \cdot 10^{-3}$	0.022
B	(2:1)	-2.37	3.845	$6.1 \cdot 10^{-3}$	0.015
			3.696	$7.0 \cdot 10^{-3}$	0.019
C	(3:3 ecl)	-3.18	3.906	$5.7 \cdot 10^{-3}$	0.014
			3.906	$5.7 \cdot 10^{-3}$	0.014
			4.489	$2.3 \cdot 10^{-3}$	$5.7 \cdot 10^{-3}$
D	(3:2)	-2.90	4.151	$4.1 \cdot 10^{-3}$	$9.7 \cdot 10^{-3}$
			4.173	$3.9 \cdot 10^{-3}$	$9.3 \cdot 10^{-3}$
			4.091	$4.2 \cdot 10^{-3}$	0.010
			4.369	$2.7 \cdot 10^{-3}$	$6.7 \cdot 10^{-3}$
E	~(3:3 sta)	-3.74	3.921	$5.8 \cdot 10^{-3}$	0.014
			3.920	$5.8 \cdot 10^{-3}$	0.014
			4.248	$3.4 \cdot 10^{-3}$	$8.4 \cdot 10^{-3}$
			4.159	$3.9 \cdot 10^{-3}$	$9.5 \cdot 10^{-3}$
F	(2:2)	-2.67	4.115	$4.3 \cdot 10^{-3}$	0.010
			4.199	$3.7 \cdot 10^{-3}$	$8.9 \cdot 10^{-3}$
			4.419	$2.6 \cdot 10^{-3}$	$6.5 \cdot 10^{-3}$
			4.199	$3.7 \cdot 10^{-3}$	$8.8 \cdot 10^{-3}$

### 3. Impact of the electrostatic component on the strength of the C-Br $\cdots$ Br-C interactions

As already mentioned, the intermolecular interactions in (CBr<sub>4</sub>)<sub>2</sub> dimers are good models for C-Br $\cdots$ Br-C interactions where the impact of the electrostatic component is minimized. However, as will be shown below also on model dimers, the impact of the electrostatic component on the C-Br $\cdots$ Br-C interaction energy cannot be ignored.

According to the multipolar expansion, the electrostatic component can be rationalized by looking at the properties of the charge-charge, charge-dipole, dipole-dipole, and the terms involving the quadrupoles (as leading terms). Thus, the larger the dipole and quadrupole of the interacting fragments, the strongest should be the electrostatic component of the dimer interaction energy. For instance, the absence of net charge and dipole is determinant to get a small electrostatic component. It is worth to remember here that in halogen $\cdots$ halogen interactions the electrostatic component also depends on the so-called  $\sigma$ -hole.<sup>17,24-28</sup>

It is possible to get a first estimation on the impact of the electrostatic component in C-Br $\cdots$ Br-C interactions by comparing the interaction energy of the (CH<sub>4-n</sub>Br<sub>n</sub>)<sub>2</sub> ( $n = 1 - 4$ ) dimers, see Table 2. These are all neutral monomers, where the change in the value of  $n$  (the degree of bromination of the molecule) triggers a change in its dipole and quadrupole moments, due to the substitution of Br atoms by less electronegative H atoms. The study was carried out at the optimum geometry of the (1:1) conformation of the four dimers (Figure 2), which only allows the formation of a single C-Br $\cdots$ Br-C short contact. Overall, the stability of the studied dimers increases with the degree of bromination of the interacting fragment (Table 2). However, such increment is proportionally much higher when going from  $n = 1$  to  $n = 2$  (where the interaction energies change from -0.70 to -0.92 kcal mol<sup>-1</sup>) than from  $n = 2$  to  $n = 3$  (where they go from -0.92 to -0.95 kcal mol<sup>-1</sup>), or from the  $n = 3$  to  $n = 4$  dimer (from -0.95 to -0.98 kcal mol<sup>-1</sup>). A SAPT evaluation of the components of the interaction energy (see also Table 2) shows that in all dimers the dispersion component is the dominant stabilizing term, followed by the induction term, and by an even smaller electrostatic component. It is also worth mentioning that the electrostatic component in the (CBr<sub>4</sub>)<sub>2</sub> dimer is 0.10 kcal mol<sup>-1</sup>, although its value should be zero according to a mono-centered second-order multipolar expansion, since the charge, dipole, and quadrupole moments of CBr<sub>4</sub> are equal to zero. This non-zero value is attributed to the interactions of the anisotropic electron densities on each interacting Br, that is, their  $\sigma$ -hole. The variation of  $E_{c1}$  along the series (CHBr<sub>3</sub>)<sub>2</sub>, (CH<sub>2</sub>Br<sub>2</sub>)<sub>2</sub>, and (CH<sub>3</sub>Br)<sub>2</sub>, can be rationalized on the basis of the variation of size and direction of the dipole induced on each fragment by the Br substitution. Finally let us remark, again, the good agreement between the MP2 and SAPT interaction energies.

**Table 2.** Interaction energy (MP2) and SAPT decomposition of the (CBr<sub>4</sub>)<sub>2</sub>, (CHBr<sub>3</sub>)<sub>2</sub>, (CH<sub>2</sub>Br<sub>2</sub>)<sub>2</sub>, and (CH<sub>3</sub>Br)<sub>2</sub> dimers on their (1:1) orientation. The BSSE was corrected. All energy values are given in kcal mol<sup>-1</sup>. Equilibrium Br $\cdots$ Br distance, dipole, and quadrupole moments of each isolated monomer are also indicated. The aug-cc-pVTZ basis set was used in the MP2 calculations of all dimers, while the SAPT analyses were performed using the aug-cc-pVTZ for the two interacting Br atoms, the aug-cc-pVDZ for the rest of Br atoms, and the cc-pVDZ for the C and H atoms.

	$r$ (Å)	$\mu$ (D)	$Q$ (D Å)	$E_{el}$	$E_{ex}$	$E_{ind}$	$E_{disp}$	$E_{int,SAPT}$	$E_{int,MP2}$
(CBr <sub>4</sub> ) <sub>2</sub>	3.47	0.0	0.0	0.10	2.51	-0.69	-2.96	-1.04	-0.98
(CHBr <sub>3</sub> ) <sub>2</sub>	3.53	1.05	2.07	-0.08	2.19	-0.50	-2.60	-0.99	-0.95
(CH <sub>2</sub> Br <sub>2</sub> ) <sub>2</sub>	3.56	1.76	4.49	-0.24	2.05	-0.37	-2.37	-0.93	-0.92
(CH <sub>3</sub> Br) <sub>2</sub>	3.60	2.20	4.01	-0.13	1.93	-0.29	-2.17	-0.65	-0.70

### 4. Angular dependence of the C-Br $\cdots$ Br-C interactions

The angular dependence of the C-Br $\cdots$ Br-C interactions was defined for the C(*ipso*) = C(sp<sup>3</sup>) case, the most common type of hybridization shown by the C(*ipso*) atoms. This angular dependence was obtained by computing the variation of the interaction energy with the  $\theta_1$  and  $\theta_2$  angles,  $E_{int}(\theta_1, \theta_2)$ , shown in Figure 6. The  $E_{int}(\theta_1, \theta_2)$  surface was only evaluated when  $\theta_1$  and  $\theta_2$  were both placed within the [90 – 180]° range, since at smaller angles undesired C-H $\cdots$ Br bonds were also formed, confirmed by doing an AIM analysis of the dimer electron density. The  $E_{int}(\theta_1, \theta_2)$  surface presents a global minimum at ( $\theta_1 = 180^\circ$ ,  $\theta_2 = 90^\circ$ ), equivalent by symmetry to the ( $\theta_1 = 90^\circ$ ,  $\theta_2 = 180^\circ$ ) minimum (or (180,90) and (90,180), according to the ( $\theta_1, \theta_2$ ) notation). These two minima are of the Type II class. A third minimum is also observed for the (90,90) orientation, a Type I orientation. On the other hand, the (150,150) orientation was commonly described as a minimum structure.<sup>19</sup> This orientation, however, is only a minimum for the restricted case of  $\theta_1 = \theta_2$  (i.e., the Type I orientations), as shown in the plot of the  $E_{int}(\theta_1 = \theta_2)$  curve (Figure 6b). According to Figure 6a, the (150,150) orientation is found to be a saddle point on the  $E_{int}(\theta_1, \theta_2)$  surface, i.e. a transition state along the pathway connecting the (180,90) and the (90,180) minima. As will be shown below, the shape of the computed  $E_{int}(\theta_1, \theta_2)$  surface agrees well with the shape of the probability of distribution of the  $\theta_1$  and  $\theta_2$  angles,  $P(\theta_1, \theta_2)$ , generated when searching for all C-Br $\cdots$ Br-C interactions presenting short-distance Br $\cdots$ Br contacts among the crystals deposited in the CSD. A similar good agreement was previously reported for C-Cl $\cdots$ Cl-C interactions.<sup>19,32</sup>

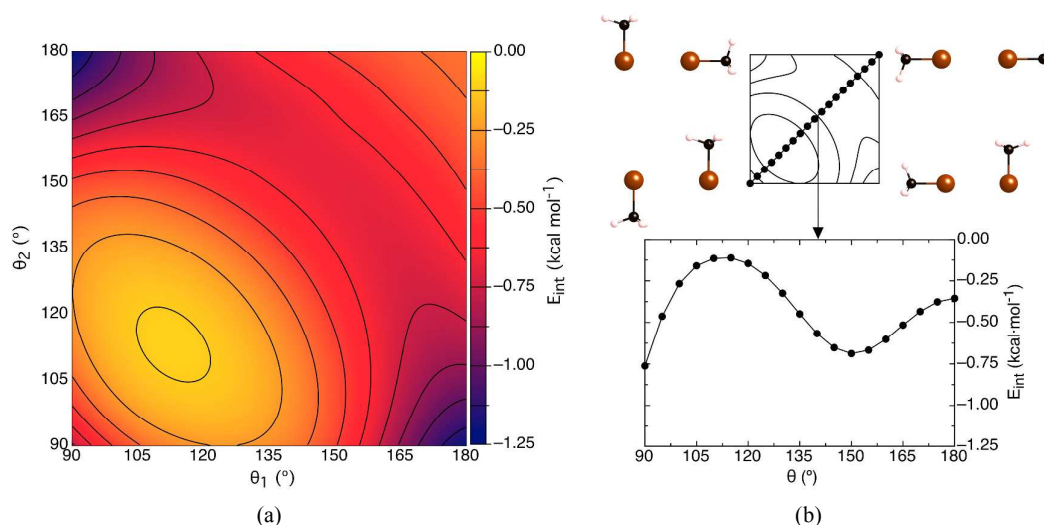


**Figure 6.** (a) Plot of the interaction energy surface as a function of the  $\theta_1$  and  $\theta_2$  angles,  $E_{\text{int}}(\theta_1, \theta_2)$ , computed at the MP2/6-311++G\*\* level for the  $(\text{CH}_3\text{Br})_2$  dimer. The BSSE was not corrected. (b) Interaction energy curve,  $E_{\text{int}}(\theta_1=\theta_2)$ , computed from the  $E_{\text{int}}(\theta_1, \theta_2)$  potential energy surface by selecting only the diagonal value (these values describe the relative stability of the Type I orientations).

The impact of the electrostatic component on determining the shape of the  $E_{\text{int}}(\theta_1, \theta_2)$  surface was initially evaluated by doing SAPT calculations on the  $(\text{CH}_3\text{Br})_2$  dimer, Table 3 (first row of each subset). The study was done on the (180,180) and (90,90) Type I orientations, as well as for the (180,90) Type II orientation. The MP2 results show that the (180,90) orientation is the most stable one among the three studied here ( $-1.44 \text{ kcal mol}^{-1}$ , while that for the other two orientations is  $-0.70$  and  $-0.88 \text{ kcal mol}^{-1}$ ). On the other hand, the SAPT components analysis for the same three orientations concludes that the higher stability of the (180,90) orientation is mostly due to a drastic increment in the electrostatic component, which varies from  $-2.09 \text{ kcal mol}^{-1}$  in the (180,90) orientation, to  $-0.13$  and  $-0.73 \text{ kcal mol}^{-1}$  in the (180,180) and (90,90), respectively. There is also an increment of the dispersion and induction terms, most likely caused by a decrease on the  $\text{Br}\cdots\text{Br}$  distance, although balanced by the increase in the repulsive character of the exchange-repulsion component (it is known that at shorter distances these three components increase, in absolute value). Hence, although the stability of  $\text{C}-\text{Br}\cdots\text{Br}-\text{C}$  interactions mostly originates from the dispersion component, the angular preference of these dimers is strongly affected by changes in the electrostatic component.

**Table 3.** Interaction energy (MP2) and SAPT decomposition of the  $(\text{CH}_3\text{Br})_2$ ,  $(\text{H}_2\text{CCHBr})_2$ ,  $(\text{C}_6\text{H}_5\text{Br})_2$ , and  $(\text{HCCBr})_2$  dimers for three  $(\theta_1, \theta_2)$  orientations. The BSSE was corrected. All energy values are given in  $\text{kcal mol}^{-1}$ . Their equilibrium  $\text{Br}\cdots\text{Br}$  distance is also indicated. The aug-cc-pVTZ basis set was used in the MP2 calculations of all dimers, while the SAPT analyses were performed using the aug-cc-pVTZ for the Br atoms and the cc-pVDZ for the C and H atoms.

	$r$ (Å)	$E_{\text{el}}$	$E_{\text{ex}}$	$E_{\text{ind}}$	$E_{\text{disp}}$	$E_{\text{int,SAPT}}$	$E_{\text{int,MP2}}$
(180,180)							
$(\text{CH}_3\text{Br})_2$	3.60	-0.13	1.93	-0.29	-2.17	-0.65	-0.70
$(\text{H}_2\text{CCHBr})_2$	3.56	-0.26	2.12	-0.33	-2.32	-0.79	-0.81
$(\text{C}_6\text{H}_5\text{Br})_2$	3.50	-0.40	2.64	-0.42	-2.70	-0.89	-0.93
$(\text{HCCBr})_2$	3.55	0.66	1.50	-0.42	-2.06	-0.31	-0.17
(180,90)							
$(\text{CH}_3\text{Br})_2$	3.56	-2.09	4.44	-0.64	-2.95	-1.24	-1.44
$(\text{H}_2\text{CCHBr})_2$	3.55	-1.88	4.25	-0.61	-3.13	-1.37	-1.55
$(\text{C}_6\text{H}_5\text{Br})_2$	3.47	-2.35	5.50	-0.81	-4.07	-1.73	-2.03
$(\text{HCCBr})_2$	3.51	-1.72	3.88	-0.74	-2.96	-1.53	-1.61
(90,90)							
$(\text{CH}_3\text{Br})_2$	3.98	-0.73	2.14	-0.24	-1.96	-0.78	-0.88
$(\text{H}_2\text{CCHBr})_2$	3.90	-0.66	2.46	-0.21	-2.36	-0.77	-0.94
$(\text{C}_6\text{H}_5\text{Br})_2$	3.76	-1.10	3.69	-0.31	-3.52	-1.24	-1.55
$(\text{HCCBr})_2$	3.84	-1.06	2.48	-0.19	-2.23	-1.01	-1.20

### 5. Impact of the C(*ipso*) hybridization on the properties of the C-Br $\cdots$ Br-C interactions

As already pointed out, the strength of the C-Br $\cdots$ Br-C interactions also depends on the hybridization of the carbon atom to which the interacting Br atoms are bonded (the C(*ipso*) atom). Such dependence is already observed in the MP2 data plotted in Figure 1, which now can be used to illustrate the impact of the C(*ipso*) hybridization on the interaction energy of the C(sp<sup>m</sup>)-Br $\cdots$ Br-C(sp<sup>m</sup>) interaction ( $m = 1 - 3$ ). In addition to the three orientations of the  $(\text{CH}_3\text{Br})_2$ ,  $(\text{H}_2\text{CCHBr})_2$ , and  $(\text{HCCBr})_2$  model dimers shown in Figure 1, the interaction energy of the  $(\text{C}_6\text{H}_5\text{Br})_2$

dimer, where  $C(ipso) = C(sp^2\text{-Aromatic})$ , was added to the study, thus covering the most usual types of hybridizations.

The interaction energy for the four aforementioned model dimers is collected in Table 3, for the (180,180), (180,90), and (90,90) orientations. These results show that for the (180,180) orientation the  $C(sp^2\text{-Ar})$  dimer is the most stable one (about  $0.1 \text{ kcal mol}^{-1}$  more stable than the  $C(sp^2)$  dimer, and  $0.2$  and  $0.8 \text{ kcal mol}^{-1}$  more stable than the  $C(sp^3)$ , and  $C(sp)$  dimers). A similar trend is observed for the (180,90) and (90,90) orientations in Table 3, although in the latter two orientations the  $C(sp)$  dimer becomes more stable than the  $C(sp^3)$  and non-aromatic  $C(sp^2)$ . It is worth noting that the (180,90) is the most stable orientation for all  $C(ipso)$  hybridizations.

The SAPT decomposition for these four dimers was evaluated for the (180,180), (180,90), and (90,90) orientations, (see also Table 3). As a general trend, all interactions are energetically stabilizing and dominated by their  $E_{ex}$  (destabilizing) and  $E_{disp}$  (stabilizing) components. The electrostatic term becomes significantly stabilizing in the (180,90) orientation, for all hybridizations, reflecting the existence of orientations where the  $\sigma$ -holes and the dipole moments cooperate.

## 6. The nature of C-Br $\cdots$ Br-C interactions found in molecular crystals deposited in the CSD

The properties of the C-Br $\cdots$ Br-C interactions have been so far evaluated in small model dimers, that is, in the  $(CH_{4-n}Br_n)_2$  ( $n = 1 - 4$ ),  $(H_2CCHBr)_2$ ,  $(C_6H_5Br)_2$ , and  $(HCCBr)_2$  dimers. In this section, the knowledge acquired on those models is complemented by the analysis of the strength of full-sized dimers extracted from the Cambridge Structural Database (CSD), presenting a sole C-Br $\cdots$ Br-C short-distance intermolecular bond. These dimers were selected by carrying out a query in the CSD searching for molecular crystals presenting C-Br $\cdots$ Br-C interactions whose Br $\cdots$ Br distance is placed within the  $3.0 - 4.5 \text{ \AA}$  range (see the Methodological details). A total of 9762 non-equivalent Br $\cdots$ Br contacts, extracted from 4182 crystals of neutral brominated molecules were found. Among these contacts, 2512 are  $C(sp^3)$  contacts, 7232 are  $C(sp^2)$  contacts (among them, 7040 are  $C(sp^2\text{-Ar})$  contacts), and 18  $C(sp)$  contacts. The distribution of Br $\cdots$ Br distances and  $(\theta_1, \theta_2)$  angles (the latter restricted to Br $\cdots$ Br distances smaller than  $3.7 \text{ \AA}$ ) for these 9762 contacts are plotted in Figure 7. The histogram reveals that the closest C-Br $\cdots$ Br-C contact is located around  $3.2 \text{ \AA}$ ,  $0.5 \text{ \AA}$  shorter than twice the bromine van der Waals radius ( $1.85 \text{ \AA}$ ), thus suggesting the stabilizing nature of these interactions. The maximum in the distance distribution is found around  $3.9 \text{ \AA}$ . The angle scattergram shows a significant preference for the Type I (i.e.,  $\theta_1 = \theta_2$ ) and Type II (i.e.,  $(\theta_1 = 90^\circ, \theta_2 = 180^\circ)$  or  $(\theta_1 = 180^\circ, \theta_2 = 90^\circ)$ ) orientations. In particular, Type I interactions, associated to the presence of inversion centers among the crystal symmetry elements, exhibit an energy minimum at *ca.*  $\theta = 150^\circ$  (Figure 6b), fact that is in good agreement with the presence of a maximum in the probability of presence in the same region of Figure 7. The curve in Figure 6b also show a maximum of energy at  $180^\circ$  as well as around  $110^\circ$ , region where the Type I interactions present minima in the probability of presence (see Figure 7). However, Figure 6 and 7 present a remarkable difference in relation to the nature of the local minimum found in the Type I curve of Figure 6b: while Figure 6a indicates that this point is a transition state, Figure 7 indicates that it is a minimum, a difference that prompted us to perform a deeper analysis of the crystal structures, which is described hereafter.

Let us start by pointing out that the distance histogram (that is, a  $(P(r_{Br\cdots Br}))$  curve) presents a shape similar to the specular reflection along the horizontal  $E_{int} = 0$  axis of the potential energy curves of Figure 3. In fact, the distance histogram (or its inverted form) can be computationally reproduced by computing the  $E_{int}$  curve for each dimer present in the histogram in the same environment found in the crystal where they are present, and then counting the number of dimers that have their minima within  $r_{Br\cdots Br}$  and  $r_{Br\cdots Br} + s$  ( $s$  being a given step size). If the number of dimers is large enough to fully reproduce the environmental effects, the computed  $(P, r_{Br\cdots Br})$  histogram indicates the probability of finding the minimum of the potential energy curve within a given range of distances for the dimers extracted from crystals. Thus, the histogram defines a sort of average potential for the C-Br $\cdots$ Br-C interactions valid for the molecular crystals included in the study, although if the subset of molecular crystals included in the study covers all types and enough representatives from each type, the average potential should work with any molecular crystal. It is worth pointing out that usually the energy scale of the y-axis is substituted by a probability of presence scale (the energetic scale could be recovered, for instance, by averaging the  $E_{int}$  for all dimers within the same step, thus getting an average  $E_{int}(Br\cdots Br)$  curve). If the computational methodology employed is accurate enough and the crystal environment has been properly reproduced, the computed  $(P, r_{Br\cdots Br})$  curve should mimic the experimental one. One can approximate the shape of the  $(P, r_{Br\cdots Br})$  curve by applying the previous process to a subset of randomly selected dimers smoothly distributed over the range of distances of interest. The analysis should be performed on a subset of crystals governed by the same class of interactions, in order to avoid misleading results.<sup>48-50</sup>

A relationship like that present between  $(P(r_{Br\cdots Br}))$  and  $E_{int}(C-Br\cdots Br-C)$  was also expected between  $P(\theta_1, \theta_2)$  and  $E_{int}(\theta_1, \theta_2)$ . Accordingly, regions where Figure 7 presents a maximum of probability should correspond to regions where Figure 6a has a minimum in energy. However, as already mentioned, such behavior does exist between Figures 6 and 7. Trying to find the reasons why in C-Br $\cdots$ Br-C interactions  $(\theta_1, \theta_2)$  and  $E_{int}(\theta_1, \theta_2)$  are not correlated, while in other interactions they present they are, we realized that: (a) Figure 6 describes the energetic preferences of an isolated dimer (in this case the  $(H_3CBr)_2$  dimer) oriented in such a way that the C-Br $\cdots$ Br-C interaction dominates the dimer interaction energy; and (b) Figure 7, describes the average preferences of many molecules presenting C-Br $\cdots$ Br-C interactions, but also other intermolecular interactions (i.e., while Figure 6 gives information on  $E_{int}(C-Br\cdots Br-C)$ , Figure 7 does it on  $E_{tot}(\theta_1, \theta_2) = E_{int}(C-Br\cdots Br-C) + E_{other}$ ), (c) thus,  $E_{tot}(\theta_1, \theta_2) \approx E_{int}(C-Br\cdots Br-C)$  in the majority of crystals present in the subset, a situation only possible when  $E_{int}(C-Br\cdots Br-C) \gg E_{other}$  (case 1) or,  $E_{other}$  is nearly constant for all  $(\theta_1, \theta_2)$  angles of interest (case 2).

In order to determine if the C-Br $\cdots$ Br-C interactions extracted from CSD crystals that have Br $\cdots$ Br distance within the  $3.0-4.5 \text{ \AA}$  range (in the following, the Br-Br-4.5 subset) belong to one of the two cases described in the last

paragraph, we have done two types of studies with the Br-Br-4.5 subset. First, for the shortest 100 contacts of the Br-Br-4.5 subset, we have characterized the crystal packing. Figure S1 shows for representative selection of the Br-Br-4.5 subset, the geometry of the dimer presenting the shortest and the next C-Br $\cdots$ Br-C interaction, or when the size of the molecule or the complexities of the C-Br $\cdots$ Br-C interactions in the crystal are not well described with a dimer plot, it shows the network of shortest C-Br $\cdots$ Br-C interactions within the crystal. We also determined the values of the most relevant geometrical parameters for the C-Br $\cdots$ Br-C interactions (Table S1, all the shortest 100 contacts have Br $\cdots$ Br distances within the 3.0-3.4 Å range). The relative importance of  $E_{\text{int}}(\text{C-Br}\cdots\text{Br-C})$  with respect to  $E_{\text{other}}$  was qualitatively estimated by comparing the number of C-Br $\cdots$ Br-C interactions that they can present among all possible intermolecular interactions. These results were supplemented with statistical analysis on the full Br-Br-4.5 subset, aimed at looking for long distance trends among the geometrical parameters of Table S1. The analysis of Figure S1 and Table S1 shows a lack of homogeneity in the Br-Br-4.5 subset (for instance, the subset includes small and highly Br-substituted molecules, together with large mono Br-substituted molecules), which also affects at the relative weight of  $E_{\text{int}}(\text{C-Br}\cdots\text{Br-C})$  with respect to  $E_{\text{other}}$ . This explains the different shape of Figure 6a and 7. Such lack of homogeneity is also manifested when looking at the trends in the geometrical variables. Thus, Table S2 collects the proportion of symmetric (i.e., those where  $\theta_1 = \theta_2$ ) and non-symmetric C-Br $\cdots$ Br-C contacts in the Br-Br-4.5 subset (such proportion can be evaluated by looking at the number of contacts that have their  $\langle\text{C-Br1}\cdots\text{Br2}$  and  $\langle\text{C-Br2}\cdots\text{Br1}$  angles equal with a difference smaller than 2 degrees). Table S2 shows that while the proportion of symmetric C-Br $\cdots$ Br-C contacts varies with the Br $\cdots$ Br distance, being about 80-100% for contacts whose Br $\cdots$ Br separation is smaller than 3.4 Å, while it goes down to 40% when the Br $\cdots$ Br cutoff distance becomes 3.7 Å.

Finally, the angular preference of the shortest C-Br $\cdots$ Br-C contacts was investigated trying to determine why they have a maximum of probability at about  $\theta_1 = \theta_2 \approx 155^\circ$ . A plot of the value of the  $\langle\text{C-Br1}\cdots\text{Br2}$  angle and the Br $\cdots$ Br distance, (Figure 2a; the same trends are observed by looking at the values of  $\langle\text{C-Br2}\cdots\text{Br1}$  angle and the Br $\cdots$ Br distance, Figure 2b) shows that at short Br $\cdots$ Br distances, where it has been shown that the contacts are mostly symmetric, the  $\langle\text{C-Br1}\cdots\text{Br2}$  angle presents a maximum of probability around  $155^\circ$ . As the Br $\cdots$ Br distance is increased, a second maximum around  $90^\circ$  builds up. As a consequence, the distribution of  $\langle\text{C-Br}\cdots\text{Br}$  angles looks like a plateau spanning the  $80$ - $160^\circ$  region (see Figure S3). A look at Figure S1 and Table S1 shows that  $\langle\text{C-Br}\cdots\text{Br}$  angles of  $180^\circ$  (or smaller than  $80^\circ$ ) are only found in sterically hindered molecules, where also each C-Br group participates in only one C-Br $\cdots$ Br-C contact. Otherwise, C-Br groups make more than one C-Br $\cdots$ Br-C short contact with adjacent molecules, bending also their  $\langle\text{C-Br}\cdots\text{Br}$  angles in order to better accommodate these contacts. One should keep in mind that crystals in the Br-Br-4.5subset also allow the simultaneously formation of intermolecular interactions other than the C-Br $\cdots$ Br-C interaction. Such a fact, added to possible steric factors, explain why the minimum of the  $\langle\text{C-Br}\cdots\text{Br}$  distribution is not found at angles close to  $90^\circ$ , where a single C-Br group optimizes the simultaneous formation of two C-Br $\cdots$ Br-C contacts.

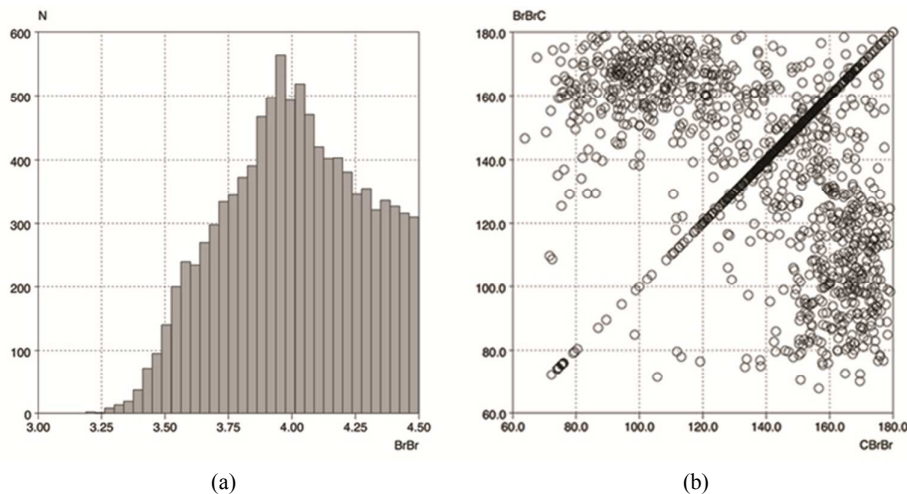


**Figure 7.** (a) Histogram showing the number of Br $\cdots$ Br contacts with the Br $\cdots$ Br distance for the C-Br $\cdots$ Br-C interactions found in the crystals deposited in CSD (see text for details). (b) Scattergram showing the values of the  $\theta_1$  and  $\theta_2$  angles for those interactions whose Br $\cdots$ Br distances is smaller or equal than 3.7 Å (twice the bromine van der Waals radius).

Based on the above considerations, a first approximation about the nature of the C-Br $\cdots$ Br-C interactions in molecular crystals can be obtained by computing the interaction energy for the 39 dimers indicated above, extracted from the 4182 molecular crystals presenting C-Br $\cdots$ Br-C intermolecular interactions in the CSD. For each dimer, the  $\theta_1$  and  $\theta_2$  angles and the  $C(\textit{ipso})$  hybridization were also reported, to ensure a proper sampling of all variables previously shown to influence the C-Br $\cdots$ Br-C strength. An AIM analysis of the interaction energy was also performed in the 39 dimers selected, in order to verify that only dimers presenting one Br $\cdots$ Br bond were included in the subset to compute. It is worth mentioning here that at distances larger than 4 Å usually more than one BCP was found and thus the number of dimers is smaller in the 4.0 - 4.5 Å region.

The 39 dimers selected for the computational evaluation of the properties of their C-Br $\cdots$ Br-C interaction are collected in Table 4, indicating their Refcode, Br $\cdots$ Br distance,  $\theta_1$  and  $\theta_2$  angles, and  $C(\textit{ipso})$  hybridization. The range

of Br $\cdots$ Br distances goes from the 3.19 to 4.34 Å (average of 3.64 Å), while the values of the  $\theta_1$  and  $\theta_2$  angles both range within 68.8 and 180.0° (average of 134.4°). Furthermore, as shown in Figure S4, they are uniformly distributed over the range of distances and angles. Also collected in Table 4 are the interaction energy of each dimer, and the characteristic properties for the Br $\cdots$ Br BCP (the density,  $\rho$ , and Laplacian,  $\nabla^2\rho$ , at the BCP) for the sole C-Br $\cdots$ Br-C bond that they present.

The variation of the dimer interaction energy as a function of the Br $\cdots$ Br distance, the  $E_{\text{int}}(\text{Br}\cdots\text{Br})$  curve, is plotted in Figure 8a. All dimers present stable interaction energies, with values within the -2.35 to -0.38 kcal mol $^{-1}$  range (average value of -1.26 kcal mol $^{-1}$ ). The most stable dimer is that found in the *KAHCEC* crystal ( $E_{\text{int}} = -2.35$  kcal mol $^{-1}$ ), a C(sp $^2$ )-Br $\cdots$ Br-C(sp $^2$ ) interaction with a Br $\cdots$ Br distance of 3.96 Å. In contrast with the above findings on small model dimers, C(sp $^2$ )-Br $\cdots$ Br-C(sp $^2$ ) interactions are not always stronger than C(sp $^3$ )-Br $\cdots$ Br-C(sp $^3$ ) interactions. In fact, the average value of the C(sp $^2$ )-Br $\cdots$ Br-C(sp $^2$ ) interactions (-1.17 kcal mol $^{-1}$ ) is smaller than the average of the C(sp $^3$ )-Br $\cdots$ Br-C(sp $^3$ ) interactions (-1.35 kcal mol $^{-1}$ ). The small number of C(sp)-Br $\cdots$ Br-C(sp) interactions does not allow any discussion about their trends. Although the dispersion of the points in the energy scale is quite large, the overall shape of the  $E_{\text{int}}(\text{Br}\cdots\text{Br})$  curve can be taken as v-shaped, the right v arm being much shorter than the left arm. It is also remarkable the large variation of interaction energy values for interactions with a similar distance, orientation, and C(*ipso*) hybridization, which suggests that the environment around the C-Br $\cdots$ Br-C interactions also plays an important role on the strength of these interactions. As a comment, the so-called strength-length correlation (i.e., the shorter the intermolecular interaction distance is, the stronger is the interaction energy) is not obeyed in C-Br $\cdots$ Br-C interactions, a failure already recognized in hydrogen bonds $^{51}$  and Cl $\cdots$ Cl interactions. $^{32}$  The last correlation analyzed here is the angular dependence of the interaction energy,  $E(\theta_1, \theta_2)$ , which is plotted in Figure 8b. The regions of higher stability in the interaction energy are: (a) those with  $\theta_1 = \theta_2 \approx 90^\circ$  (a particular case of Type I orientations), and (b) those close to the minima for the Type II orientations. These results match the trends extracted from the calculations on model dimers, Figure 6, and are also in good agreement with the scattergram plotted in Figure 7. In summary, it can be concluded that Br $\cdots$ Br interactions are highly anisotropic.

**Table 4.** BSSE-corrected interaction energies computed at the MP2/aug-cc-pVDZ level (given in kcal mol $^{-1}$ ) for the 39 dimers extracted from the CSD, all presenting Br $\cdots$ Br distances within the 3.0 – 4.5 Å range. The Refcode of the crystal where they are present is also given, together with the Br $\cdots$ Br distance (in Å), the  $\theta_1$  and  $\theta_2$  angles (in degrees), and the hybridization of the C(*ipso*). The density (in a.u.) and Laplacian (in a.u.) of the Br $\cdots$ Br bond critical point are also given, obtained from an AIM analysis of the dimer wavefunction.

Refcode	r	$\theta_1$	$\theta_2$	C( <i>ipso</i> ) hyb.	$\rho$	$\nabla^2\rho$	$E_{\text{int}}$
TPHMBR02	3.193	180.0	180.0	sp $^3$	0.013	0.046	-0.72
QAQLUQ	3.291	144.2	162.2	sp $^2$	0.013	0.041	-0.42
QALWQQ <sup>a</sup>	3.292	162.9	162.9	sp $^2$	0.011	0.039	-0.38
YIHDEY	3.301	166.6	166.6	sp $^3$	0.011	0.037	-1.05
BAWJAL	3.312	151.2	155.7	sp $^2$	0.011	0.039	-0.56
IFOKOD	3.372	164.8	164.8	sp $^3$	9.7·10 $^{-3}$	0.033	-0.60
LIKFIU	3.390	174.0	137.4	sp $^3$	0.010	0.034	-0.95
QAQNEB	3.400	164.1	164.1	sp $^2$	8.7·10 $^{-3}$	0.031	-1.01
YAKXAJ	3.403	153.4	153.4	sp $^2$	9.3·10 $^{-3}$	0.031	-0.51
SATHIF	3.411	161.6	161.6	sp $^2$	9.4·10 $^{-3}$	0.030	-1.12
DEWYEK	3.430	142.7	142.7	sp $^2$	9.9·10 $^{-3}$	0.032	-0.77
YORYAF	3.431	158.7	158.7	sp $^3$	8.0·10 $^{-3}$	0.028	-1.75
VAGTUS	3.434	149.7	149.7	sp $^2$	9.0·10 $^{-3}$	0.030	-1.09
MAPGUG	3.496	152.0	152.0	sp $^2$	8.2·10 $^{-3}$	0.026	-1.45
INUGED	3.500	173.5	112.8	sp $^2$	8.7·10 $^{-3}$	0.028	-1.16
VUPYAH	3.521	165.4	165.4	sp $^3$	9.0·10 $^{-3}$	0.028	-0.87
JINYOV	3.527	102.4	169.8	sp $^3$	8.4·10 $^{-3}$	0.029	-1.79
ESUYEW	3.542	128.9	165.1	sp $^2$	7.8·10 $^{-3}$	0.025	-1.15
XAYKUE	3.563	140.6	140.6	sp $^3$	8.6·10 $^{-3}$	0.025	-1.16
HAMBUT	3.567	143.8	143.8	sp $^3$	7.8·10 $^{-3}$	0.024	-1.13
QERVIS	3.573	154.4	154.4	sp $^3$	6.8·10 $^{-3}$	0.022	-1.57
KAWPUU	3.587	135.3	135.3	sp $^3$	6.8·10 $^{-3}$	0.020	-0.77
IGEHIM	3.637	105.3	169.7	sp $^2$	7.2·10 $^{-3}$	0.021	-1.64
BAGWOW	3.639	98.0	164.0	sp $^2$	7.3·10 $^{-3}$	0.022	-1.39
SITQAN	3.668	141.3	141.3	sp $^2$	6.7·10 $^{-3}$	0.020	-1.09
GIYXOB	3.747	81.2	129.4	sp $^2$	7.4·10 $^{-3}$	0.019	-1.59
IZAMUR	3.752	77.4	161.9	sp $^3$	6.2·10 $^{-3}$	0.018	-1.31
BMOPCO	3.793	83.8	173.2	sp $^3$	5.7·10 $^{-3}$	0.016	-2.33
ASAXOI	3.832	165.7	89.9	sp $^2$	6.2·10 $^{-3}$	0.018	-1.79
BENBCL	3.837	116.6	116.6	sp $^3$	6.6·10 $^{-3}$	0.017	-1.36
TASWOZ	3.929	150.7	99.5	sp $^3$	5.1·10 $^{-3}$	0.013	-1.98
VOQYUM	3.942	163.5	95.0	sp $^2$	5.2·10 $^{-3}$	0.012	-1.40
KAHCEC	3.959	73.5	73.5	sp $^3$	5.4·10 $^{-3}$	0.014	-2.35
FUQJIK	3.990	130.8	130.8	sp $^2$	3.9·10 $^{-3}$	0.010	-1.38

<i>MEDMAK</i>	4.057	162.2	162.2	sp <sup>3</sup>	2.9·10 <sup>-3</sup>	8.5·10 <sup>-3</sup>	-0.56
<i>BCACEN</i>	4.061	68.8	68.8	sp	4.5·10 <sup>-3</sup>	0.012	-1.79
<i>YUYLOT</i>	4.113	77.5	77.5	sp <sup>2</sup>	4.3·10 <sup>-3</sup>	0.011	-2.00
<i>FERRUQ</i>	4.246	85.0	120.6	sp <sup>3</sup>	3.5·10 <sup>-3</sup>	8.4·10 <sup>-3</sup>	-2.05
<i>NATMIE</i>	4.430	90.4	90.4	sp <sup>2</sup>	2.6·10 <sup>-3</sup>	6.4·10 <sup>-3</sup>	-1.40

<sup>a</sup> The 6-31+G(d) basis set was used on the vanadium atoms.

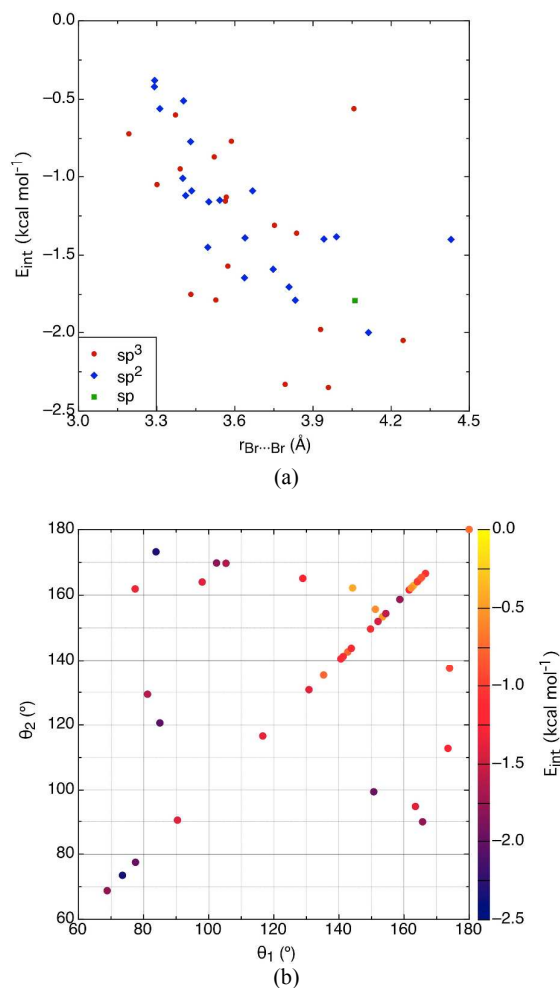


**Figure 8.** Variation of the interaction energy of the C-Br...Br-C contacts of Table 4 as a function of the Br...Br distance (a) and  $\theta_1$  angles (b), obtained at the MP2/aug-cc-pVDZ level (BSSE corrected values). The hybridization of the C(*ipso*) is also indicated in the distance plot, by the color code of each point.

Finally, we analyzed the results of the AIM study of these dimers. As already mentioned, all dimers included in Table 4 present one C-Br...Br-C intermolecular bond, associated to one Br...Br bond critical point (BCP). No other intermolecular BCP should be present, which is confirmed by the AIM analysis. As shown in Table 4 and Figure 9, the electron density ( $\rho$ ) and the Laplacian ( $\nabla^2 \rho$ ) at the BCP decrease as the Br...Br distance increases, a trend previously reported in other intermolecular interactions.<sup>30,33,52</sup> The assumption that a higher electron density at the BCP implies stronger bond energies<sup>30,53</sup> is shown to be wrong for the Br...Br BCPs found in these C-Br...Br-C interactions. Instead, the density at the BCP decreases exponentially with the Br...Br distance (Figure 9), whereas the interaction energy is v-shaped (Figure 8a), thus failing to fulfill a direct correlation between  $E_{\text{int}}$  and  $\rho_{\text{BCP}}$ . This failure was previously observed in C-Cl...Cl-C interactions.<sup>52</sup>

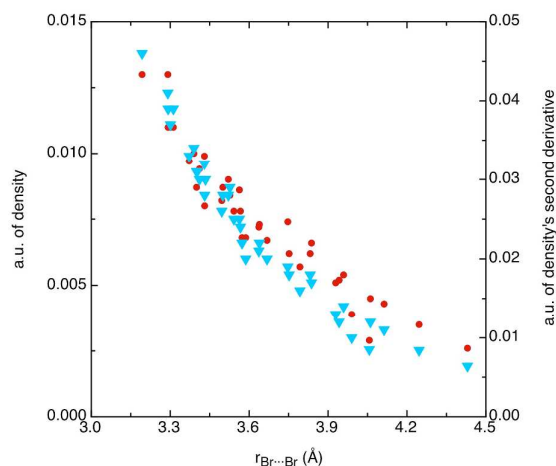


**Figure 9.** Variation of the characteristic properties of the Br...Br BCP of Table 4 as a function of the Br...Br distance. Density ( $\rho$ ) is shown in red circles (left axis) and Laplacian ( $\nabla^2 \rho$ ) is shown in light blue triangles (right axis).

## CONCLUSIONS

The nature of the C-Br...Br-C intermolecular interactions was evaluated, at the MP2/aug-cc-pVTZ level, on small model dimers and on full-sized dimers extracted from crystals deposited in the CSD. The study was structured in the following sections: (a) assessment of the selected methodology, for three orientations of the  $(\text{CH}_3\text{Br})_2$ ,  $(\text{H}_2\text{CCHBr})_2$ , and  $(\text{HCCBr})_2$  dimers, comparing the MP2/aug-cc-pVTZ results against the MP2/CBS benchmark results; (b) evaluation of the nature of the C-Br...Br-C interactions in the  $\text{CBr}_4$  crystal; (c) impact of the electrostatic component of the interaction energy on the nature of the C-Br...Br-C interactions; (d) determination of the angular dependence of the C-Br...Br-C interactions; (e) impact of the *C(ipsa)* hybridization on C-Br...Br-C interactions; and (f) study of the nature of the C-Br...Br-C interactions present in full-sized dimers of molecular crystals reported in the CSD.

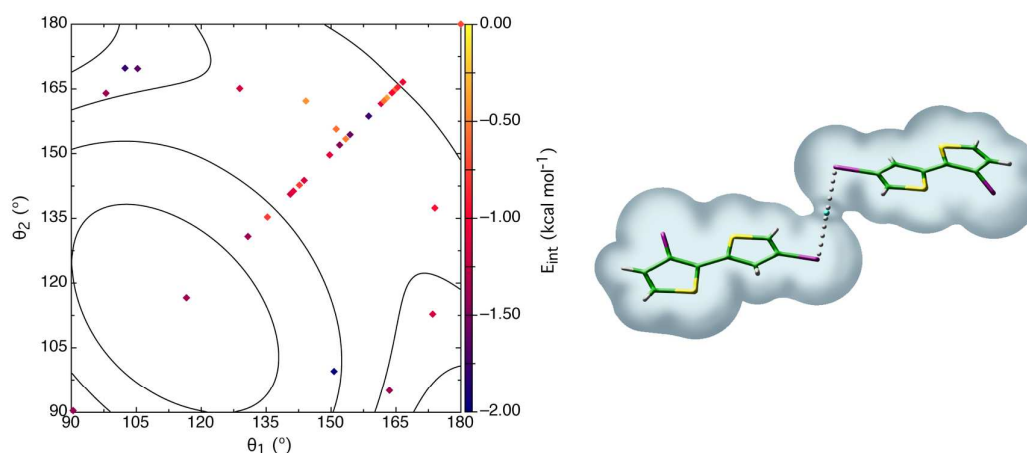
The initial MP2/CBS benchmark was done for three orientations of the  $(\text{CH}_3\text{Br})_2$ ,  $(\text{H}_2\text{CCHBr})_2$ , and  $(\text{HCCBr})_2$  dimers. The MP2/CBS interaction energy of these dimers was estimated to be -1.72, -1.83, and -1.91 kcal mol<sup>-1</sup>, respectively, at the most stable orientation of these dimers, the so-called Type II interaction (i.e.,  $\theta_i = 180^\circ$  and  $\theta_j = 90^\circ$ , where  $\theta_i$  and  $\theta_j$  arbitrary indicate the  $\langle \text{C-Br}_1 \cdots \text{Br}_2 \rangle$  and  $\langle \text{Br}_1 \cdots \text{Br}_2 \cdots \text{C} \rangle$  angles). These results also demonstrated that MP2/aug-cc-pVDZ and MP2/aug-cc-pVTZ calculations predict the same relative stability trends than MP2/CBS calculations, with a systematic energy shift of  $\sim 0.6$  kcal mol<sup>-1</sup> and  $\sim 0.2$  kcal mol<sup>-1</sup>, respectively.

Calculations on  $(\text{CBr}_4)_2$  dimers showed that, as the fragments present no dipole nor quadrupole moment, the  $\text{CBr}_4 \cdots \text{CBr}_4$  interaction energy is mostly dominated by the dispersive component. The relative orientation of the two interacting C-Br groups also affects the  $\text{CBr}_4 \cdots \text{CBr}_4$  interaction energy. When the interacting fragments present a permanent dipole, as is the case of the  $(\text{CH}_{4-n}\text{Br}_n)_2$  model dimers ( $n = 1 - 4$ ), the dispersion component of the interaction energy is still the dominating attractive component, but the electrostatic component can be as large as 70% of the dispersion. The  $E_{el}$  term can be either stabilizing or destabilizing depending on the orientation of the dipoles and  $\sigma$ -hole of the interacting fragments.

Model dimer calculations also evidenced the higher stability of  $\text{C}(\text{sp}^2\text{-Ar})\text{-Br} \cdots \text{Br}\text{-C}(\text{sp}^2\text{-Ar})$  than other hybridizations, although the order of stability with respect to these other hybridizations depended on the relative orientation of the model dimers. The angular dependence of the interaction energy was investigated by computing the  $E_{int}(\theta_1, \theta_2)$  surface on the  $(\text{CH}_3\text{Br})_2$  model dimer. Its  $E_{int}(\theta_1, \theta_2)$  surface showed that the  $150^\circ$  Type I orientation can be considered a saddle point of the conversion between the  $(180, 90)$  and  $(90, 180)$  Type II minima. The C-Br...Br-C interactions were found to be anisotropic.

Finally, the study of C-Br...Br-C interactions in dimers found in molecular crystals deposited in the CSD showed that these interactions have interaction energies that vary within the -2.35 to -0.38 kcal mol<sup>-1</sup> range (their average value of -1.26 kcal mol<sup>-1</sup>). On the other hand, they present a maximum probability of presence at 3.9 Å. The angle distribution, restricted to sub-van der Waals interactions, showed preferred orientations that matched the minima found in the  $E_{int}(\theta_1, \theta_2)$  surface computed on the  $(\text{CH}_3\text{Br})_2$  dimer. Among all these dimers, 39 dimers were selected for presenting a sole C-Br...Br-C intermolecular bond with a Br...Br distance smoothly distributed within the 3.0 – 4.5 Å range. The average value of the C-Br...Br-C interaction energy in dimers presenting a  $\text{C}(\text{sp}^3)$  hybridizations is -1.35 kcal mol<sup>-1</sup>, whereas in those having a  $\text{C}(\text{sp}^2)$  hybridization (aromatic and non-aromatic) is -1.17 kcal mol<sup>-1</sup>, in sharp contrast with the results obtained on the model dimers. This evidences that the crystal environment also affects the strength of the C-Br...Br-C interactions. A correlation between  $E_{int}$  and  $\rho_{BCP}$  proposed in the literature was found to fail in C-Br...Br-C interactions. Finally, the strength-length correlation is not fulfilled by C-Br...Br-C interactions.

## TABLE OF CONTENTS



An exhaustive theoretical study of the nature of the C-Br...Br-C interactions has been done, combining MP2/aug-cc-pVTZ evaluations of the interaction energy, Atoms-in-Molecules analysis of bonds, and SAPT energy decompositions of interaction energy. The study was done on model dimers and on dimers extracted from molecular crystals deposited in the Cambridge Structural Database.

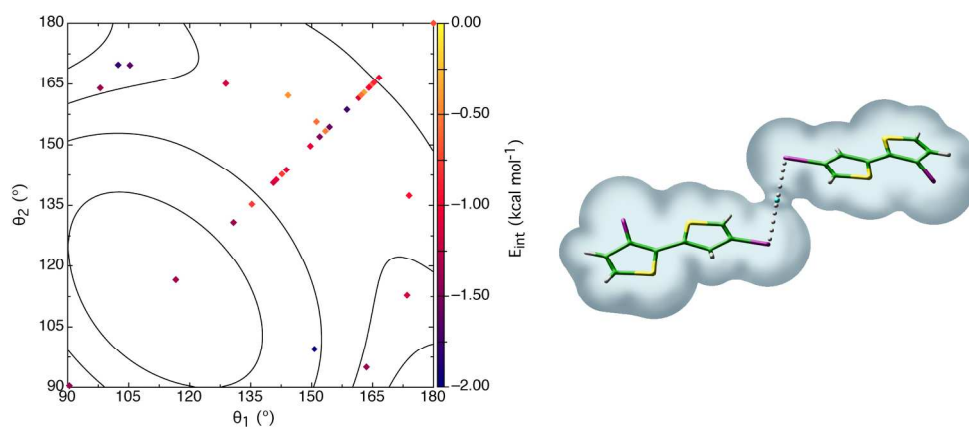
## ACKNOWLEDGEMENTS

The work was financially supported by the Ministerio de Economía y Competividad (MINECO) of the Spanish Government (MAT2011-25972, partially financed by FEDER funds) and Generalitat de Catalunya (2014 SGR 1422). We also thank CSUC and BSC for their generous allocation of computer time in their facilities.

## REFERENCES

1. G. R. Desiraju, *J. Chem. Sci.*, 2010, **122**, 667.
2. G. R. Desiraju, *J. Am. Chem. Soc.*, 2013, **135**, 9952.
3. G. A. Jeffrey, *An Introduction to Hydrogen Bonding*, Oxford University Press, 1997.
4. S. Scheiner, *Hydrogen Bonding: A Theoretical Perspective*, Oxford University Press, 1997.
5. W. C. Hamilton and J. A. Ibers, *Hydrogen bonding in solids*, W. A. Benjamin, Inc., 1968.
6. G. R. Desiraju, *The weak hydrogen bond in structural chemistry and biology*, Oxford University Press, 1990.
7. E. D'Oria and J. J. Novoa, *CrystEngComm*, 2008, **10**, 423.
8. D. Braga and F. Grepioni, *New J. Chem.*, 1998, **22**, 1159.
9. P. Metrangolo, H. Neukirch, T. Pilati, and G. Resnati, *Acc. Chem. Res.*, 2005, **38**, 386.
10. R. B. Walsh, C. W. Padgett, P. Metrangolo, G. Resnati, T. W. Hanks, and W. T. Pennington, *Cryst. Growth Des.*, 2001, **1**, 165.
11. C. A. Hunter and J. K. M. Sanders, *J. Am. Chem. Soc.*, 1990, **112**, 5525.
12. G. R. Desiraju and A. Gavezzotti, *J. Chem. Soc. Chem. Commun.*, 1989, 621.
13. S. Tsuzuki, K. Honda, T. Uchimaru, M. Mikami, and K. Tanabe, *J. Am. Chem. Soc.*, 2002, **124**, 104.
14. K. Yamasaki, *J. Phys. Soc. Japan*, 1962, **17**, 1262.
15. S. C. Nyburg, *J. Chem. Phys.*, 1964, **40**, 2493.
16. I. H. Hillier, *J. Chem. Phys.*, 1967, **46**, 3881.
17. N. Ramasubbu, R. Parthasarathy, and P. Murray-Rust, *J. Am. Chem. Soc.*, 1986, **108**, 4308.
18. G. R. Desiraju and R. Parthasarathy, *J. Am. Chem. Soc.*, 1989, **111**, 8725.
19. F. F. Awwadi, R. D. Willett, K. A. Peterson, and B. Twamley, *Chem. - Eur. J.*, 2006, **12**, 8952.
20. T. T. T. Bui, S. Dahaoui, C. Lecomte, G. R. Desiraju, and E. Espinosa, *Angew. Chem. Int. Ed.*, 2009, **48**, 3838.
21. J. A. R. P. Sarma and G. R. Desiraju, *Acc. Chem. Res.*, 1986, **19**, 222.
22. S. K. Nayak, M. K. Reddy, T. N. G. Row, and D. Chopra, *Cryst. Growth Des.*, 2011, **11**, 1578.
23. E. Bosch and C. L. Barnes, *Cryst. Growth Des.*, 2002, **2**, 299.
24. P. Politzer, J. S. Murray, and T. Clark, *Phys. Chem. Chem. Phys.*, 2013, **15**, 11178.
25. D. E. Williams and L. Y. Hsu, *Acta Crystallogr. Sect. A*, 1985, **41**, 296.
26. S. C. Nyburg and W. Wong-Ng, *Proc. R. Soc. A Math. Phys. Eng. Sci.*, 1979, **367**, 29.
27. S. C. Nyburg and W. Wong-Ng, *Inorg. Chem.*, 1979, **18**, 2790.
28. S. L. Price, A. J. Stone, J. Lucas, R. S. Rowland, and A. E. Thomleytj, *J. Am. Chem. Soc.*, 1994, **116**, 4910.
29. T. Clark, M. Hennemann, J. S. Murray, and P. Politzer, *J. Mol. Model.*, 2007, **13**, 291.

30. M. V Vener, A. V Shishkina, A. A. Rykounov, and V. G. Tsirelson, *J. Phys. Chem. A*, 2013, **117**, 8459.
31. V. R. Hathwar and T. N. Guru Row, *J. Phys. Chem. A*, 2010, **114**, 13434.
32. M. Capdevila-Cortada, J. Castelló, and J. J. Novoa, *CrystEngComm*, 2014, **16**, 8232.
33. R. M. Osuna, V. Hernández, J. T. L. Navarrete, E. D'Oria, and J. J. Novoa, *Theor. Chem. Acc.*, 2010, **128**, 541.
34. T. Helgaker, W. Klopper, H. Koch, and J. Noga, *J. Chem. Phys.*, 1997, **106**, 9639.
35. A. Halkier, T. Helgaker, P. Jørgensen, W. Klopper, H. Koch, J. Olsen, and A. K. Wilson, *Chem. Phys. Lett.*, 1998, **286**, 243.
36. S. F. Boys and F. Bernardi, *Mol. Phys.*, 1970, **19**, 553.
37. Gaussian03, Revision E.01, M. J. Frisch, G. W. Trucks, H. B. Schlegel, G. E. Scuseria, M. A. Robb, J. R. Cheeseman, G. Scalmani, V. Barone, B. Mennucci, G. A. Petersson, H. Nakatsuji, M. Caricato, X. Li, H. P. Hratchian, A. F. Izmaylov, J. Bloino, G. Zheng, J. L. Sonnenberg, M. Hada, M. Ehara, K. Toyota, R. Fukuda, J. Hasegawa, M. Ishida, T. Nakajima, Y. Honda, O. Kitao, H. Nakai, T. Vreven, J. E. Montgomery, Jr. A., Jr. Peralta, F. Ogliaro, M. Bearpark, J. J. Heyd, E. Brothers, K. N. Kudin, R. Staroverov, V. N. Kobayashi, J. Normand, K. Raghavachari, A. Rendell, J. C. Burant, S. S. Iyengar, J. Tomasi, M. Cossi, N. Rega, N. J. Millam, M. Klene, J. E. Knox, J. B. Cross, V. Bakken, C. Adamo, J. Jaramillo, R. Gomperts, R. E. Stratmann, O. Yazyev, A. J. Austin, R. Cammi, C. Pomelli, J. W. Ochterski, R. L. Martin, K. Morokuma, V. G. Zakrzewski, G. A. Voth, P. Salvador, J. J. Dannenberg, S. Dapprich, A. D. Daniels, Ö. Farkas, J. B. Foresman, J. V. Ortiz, J. Cioslowski, and D. J. Fox, Gaussian Inc., Wallingford, 2003.
38. B. Jeziorski, I. Robert, and K. Szalewicz, *Chem. Rev.*, 1994, **94**, 1887.
39. J. Wu, H. Yan, Y. Jin, H. Chen, G. Dai, A. Zhong, and F. Pan, *J. Mol. Struct. THEOCHEM*, 2009, **911**, 132.
40. R. Bukowski, W. Cencek, P. Jankowski, B. Jeziorski, M. Jeziorska, S. A. Kucharski, V. F. Lotrich, A. J. Misquitta, R. Moszynski, K. Patkowski, R. Podeszwa, S. Rybak, K. Szalewicz, H. L. Williams, R. J. Wheatley, P. E. S. Wormer, and P. S. Zuchowski, *SAPT2008: An Ab Initio Program for Many-Body Symmetry-Adapted Perturbation Theory Calculations of Intermolecular Interaction Energies*.
41. R. F. W. Bader, *Atoms in Molecules: A Quantum Theory*, Oxford University Press, 1994.
42. F. W. Biegler-König, R. F. W. Bader, and T.-H. Tang, *J. Comput. Chem.*, 1982, **3**, 317.
43. F. H. Allen, *Acta Crystallogr. Sect. B Struct. Sci.*, 2002, **58**, 380.
44. S. Tsuzuki, A. Wakisaka, T. Ono, and T. Sonoda, *Chem. - Eur. J.*, 2012, **18**, 951.
45. S. J. Grabowski, *Chem. - Eur. J.*, 2013, **19**, 14600.
46. P. Metrangola, F. Meyer, T. Pilati, G. Resnati, and G. Terraneo, *Angew. Chem. Int. Ed.*, 2008, **47**, 6114.
47. J. D. Dunitz and A. Gavezzotti, *Acc. Chem. Res.*, 1999, **32**, 677.
48. D. Braga, E. D'Oria, F. Grepioni, F. Mota, J. J. Novoa, and C. Rovira, *Chem. - Eur. J.*, 2002, **8**, 1173.
49. E. D'Oria and J. J. Novoa, *CrystEngComm*, 2004, **6**, 367.
50. E. D'Oria and J. J. Novoa, *J. Phys. Chem. A*, 2011, **115**, 13114.
51. E. Espinosa, E. Molins, and C. Lecomte, *Chem. Phys. Lett.*, 1998, **285**, 170.
52. I. Mata, I. Alkorta, E. Molins, and E. Espinosa, *Chem. - Eur. J.*, 2010, **16**, 2442.
53. D. Chopra, *J. Phys. Chem. A*, 2012, **116**, 9791.



The properties of C-Br...BR-C interactions have been determined by doing MP2 theoretical calculations on model dimers and on dimers taken from the Cambridge Crystallographic Database (presenting Br...Br distances within the 3.0 to 4.5 Å range)  
283x127mm (200 x 200 DPI)